THE ASTROPHYSICAL JOURNAL, 189:569–575, 1974 May 1

ON THE UPPER ATMOSPHERE OF NEPTUNE

J. VEVERKA, L. WASSERMAN, AND CARL SAGAN
Laboratory for Planetary Studies, Cornell University, Ithaca, New York, 14850
Received 1973 June 22; revised 1973 October 29

ABSTRACT

We have reanalyzed the Mount Stromlo observations of the occultation of BD−17°4388 by Neptune and find that the upper atmosphere is not isothermal as suggested by Freeman and Lyngå. For a pure hydrogen atmosphere, our results give a temperature of 135° K at a number density of 10^{15} cm^{-3}. Above this level the possibility of a small overall positive temperature gradient is suggested by the data. The temperature structure is complicated in detail, with local 5°–10° K fluctuations some 10 km in extent associated with the numerous spikes in the light curve. Concentrations of helium greater than 50 percent can probably be ruled out.

Subject headings: abundances, planetary — atmospheres, planetary — Neptune

I. INTRODUCTION

The 1968 occultation of BD−17°4388 by Neptune was observed photoelectrically at Mount Stromlo in Australia, and at two sites in Japan. The fullest analysis of the Japanese results—at both immersion and emersion—is that of Kovalevsky and Link (1969), while the fullest treatment of the Australian observations—emersion only—is given by Freeman and Lyngå (1970). Unfortunately, the conclusions of the two groups do not agree. Kovalevsky and Link find a nonisothermal atmosphere with local scale heights, on emersion, ranging from about 50 to 64 km, while Freeman and Lyngå are satisfied with an isothermal fit to their data using a scale height of 28.9 km.

The purpose of this paper is to show that a more realistic analysis of the Australian data is possible which leads to conclusions about Neptune's upper atmosphere rather different from those reached by Freeman and Lyngå. A correct analysis of the Australian observations is essential since they are probably the best observations of the emersion event, and such occultations occur rarely.

Basically two methods for reducing occultation light curves are available. In the first, a model light curve—usually based on an isothermal model atmosphere—is fitted to the observed light curve (Baum and Code 1953; Freeman and Lyngå 1970). In the second, the light curve is inverted to calculate the refractivity profile as a function of height (Kovalevsky and Link 1969; Hubbard *et al.* 1972). The latter method is also commonly employed in the interpretation of spacecraft microwave occultation events. Wasserman and Veverka (1973) have shown that the first method cannot be applied meaningfully in the case of occultation light curves dominated by spikes, whereas in all cases the inversion method works well.

Since the occultation curve of the Neptune event is dominated by spikes, the first method cannot give a meaningful result. In fact, it is not even clear in what sense Freeman and Lyngå's isothermal curve (fig. 1, bottom, dashed curve) can be claimed to "fit" the observations.

Our first task will be to obtain a good fit using the inversion method. The procedure used here is similar to that adopted by Kovalevsky and Link (1969) in the analysis of the Japanese data. Unfortunately, Kovalevsky and Link invert not the actual observed occultation curve, spikes and all, but only what they refer to as a "mean curve." In this "mean curve" the spikes have been smoothed out by some unspecified averaging process. Ignoring spikes cannot be fully justified, and we suspect that the refractivity profiles obtained by Kovalevsky and Link, although essentially correct, do not extract the full information available in the Japanese occultation curves.

II. THE REFRACTIVITY PROFILE

Figure 1 (bottom) shows the intensity record of the emersion of BD−17°4388 from behind Neptune, as observed by Freeman and Lyngå (1969, 1970) with a *V*-filter using the Mount Stromlo 125-cm reflector. Also shown in this figure is their accepted fit to the data—a light curve corresponding to an isothermal atmosphere with a scale height of 28.9 km. Only loosely can it be said to "fit" the observations. Above the observed curve (fig. 1, top) is shown a synthetic occultation curve we have generated using the refractivity profile labeled II in figure 2. This profile was calculated by "inverting" the light curve shown in figure 1 using standard techniques discussed by Kovalevsky and Link (1969), Hubbard *et al.* (1972), and Wasserman and Veverka (1973), techniques outlined in Appendix A. This light curve is that published by Freeman and Lyngå (1970).

At the time of the occultation the Earth-Neptune distance was 29.53 a.u. The velocity of Neptune relative to the Mount Stromlo site was $v_0 = 17.95$ km s^{-1}. Using the astrometry of the event published by Freeman and Lyngå (1970), we find that the star came out in a direction 29°.5 from the normal to the limb; therefore, the component of the emersion velocity normal to the limb was $v_e = v_0 \cos(29°.5) = 15.7$ km s^{-1}. This is the value used in our calculations. For the radius of Neptune we have used 25,000 km, consistent with the findings of Kovalevsky and Link

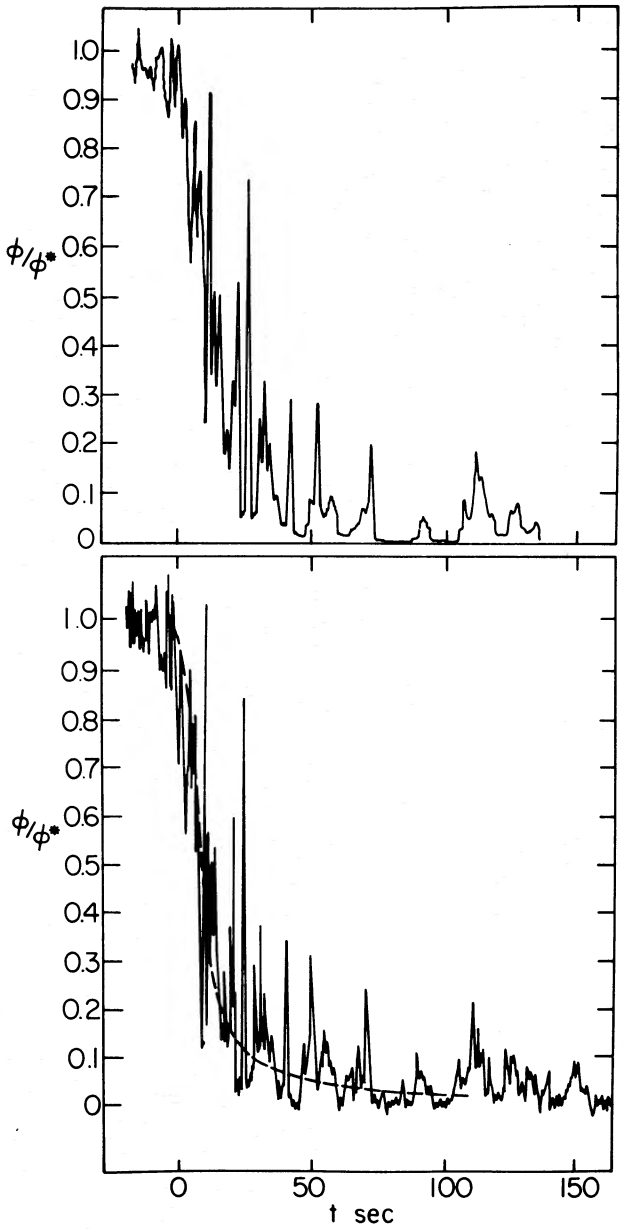

FIG. 1.—*Bottom*, Emersion light curve for the occultation of BD−17°4388 by Neptune (Freeman and Lyngå 1970). Superposed (*dashed*) is the isothermal atmosphere light curve fitted by Freeman and Lyngå to their data. *Top*, Synthetic light curve generated using refractivity profile (II) shown in fig. 2.

(1969) and Freeman and Lyngå (1970). This corresponds to a value of $g = 1090$ cm s^{-2}.

Also shown in figure 2 is the refractivity profile (labeled I) obtained by inverting the original chart recording trace of the event, from which the published light curve was prepared. This trace, a facsimile of which was kindly provided to us by Dr. K. C. Freeman agrees very closely with the curve published by Freeman and Lyngå (1970). The difference between the two refractivity profiles shown in figure 2 is attributable almost entirely to uncertainties in reading values from the two versions of the emersion record near the level of negligible refraction. Small differences in this part of the curve significantly affect the inferred refractivity profiles near the beginning of the calculations. Such reading errors could be avoided entirely by recording observations in digital form.

It is important to realize that these reading errors do not affect significantly the *meaningful* parts of the refractivity profiles. The calculated profiles cannot converge to correct values for about 3 or 4 scale heights from the beginning of the calculation (Appendix A); this uncertain part of the curves is shown dashed in figure 2. The reason for this uncertainty is that zero refractivity is assumed above the level at which the calculation begins, whereas, in fact, this cannot be true. Note that the upper portions of the two profiles in figure 2 agree very closely with each other, as do the fine details of the entire curves. The conclusion is that below the 10^{-10} refractivity level the two profiles agree closely. The quasi-linear portions of the two profiles give approximate scale heights of 55 and 58 km for curves I and II, respectively.

This quasi-scale height $\tilde{H} = 55$–58 km has been used to estimate the distance over which the refractivity profiles are uncertain: 4 scale heights $\simeq$ 240 km. This is the portion shown dashed in figure 2.

As stated above, we believe that the slight differences between curves I and II in figure 2 are due largely to uncertainties in graph reading. Since curve I is based on a facsimile of the original trace while curve II derives from a published graph based on the original trace, we tend to assign greater weight to the former in what follows.

Note that nowhere is the atmosphere truly isothermal, as evidenced by the numerous wiggles in the refractivity profiles. The quasi-linear portions give approximate scale heights of 55–58 km, and not 28.9 km, the value favored by Freeman and Lyngå.

The nonlinear nature of the refractivity profile is seen more clearly in figure 3, which shows expanded sections of the upper portions of curve II in figure 2. The bumps in this profile correspond to spikes in the light curve.

In this discussion it is assumed that spikes are due to small density fluctuations in the vertical structure of the atmosphere as proposed by Freeman and Lyngå (1970). In seeking a solution by inversion it is implicitly assumed that ray crossing is negligible. This amounts to saying that the spikes really occur at the level in the atmosphere indicated by their position on the occultation curve. Since the spikes translate into very small fluctuations in the refractivity profile, this is a reasonable assumption, and the inferred refractivity profile is probably essentially correct even if some of the spikes are due to ray crossing. At any rate, in this case there is no way in which ray crossing can be dealt with explicitly, and the assumption that it is negligible is unavoidable.

It is difficult to compare our results with those of

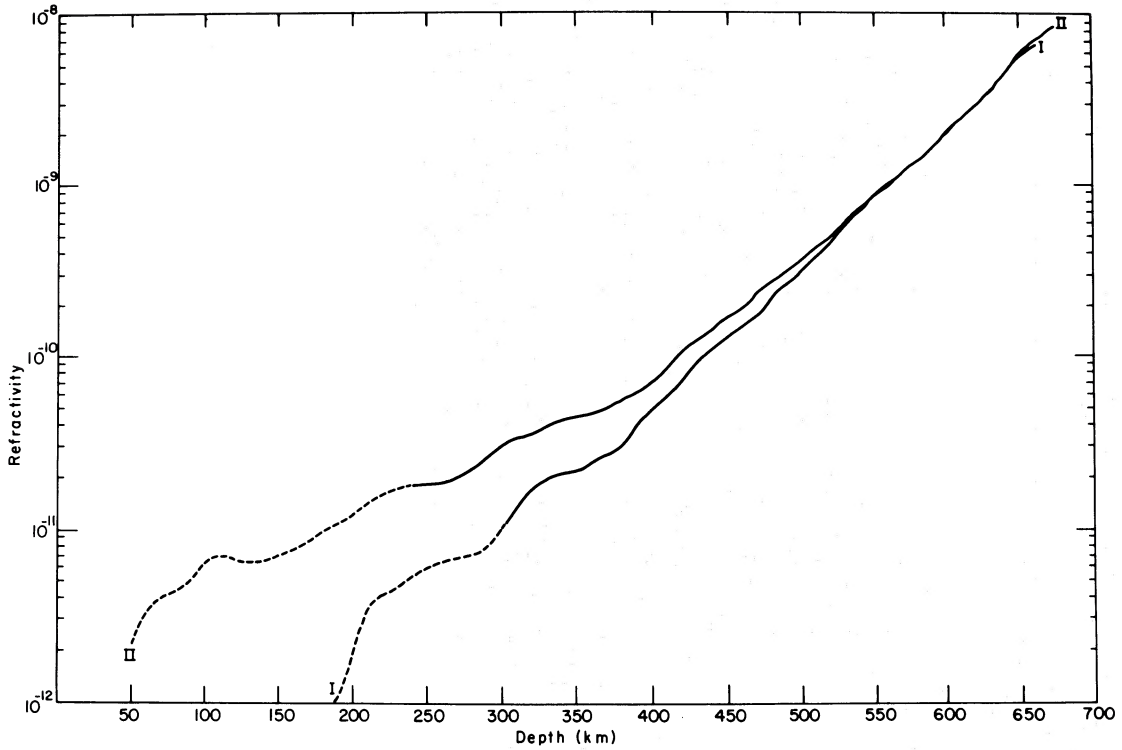

FIG. 2.—Refractivity of Neptune's upper atmosphere obtained by inverting two versions of the Mount Stromlo occultation light curve: (I) a facsimile of the chart recorder trace, and (II) the published light curve (fig. 1, bottom). The differences in the calculated profiles are attributable to uncertainties in graph reading. The zero of the depth scale is arbitrary, with the zero corresponding to the beginning point of the calculations. The depth (z) is measured inward, toward the center of Neptune. The upper portions of the curve, shown dashed, are affected by the assumed boundary condition (Appendix A). The refractivity ν is the real part of the refractive index minus one.

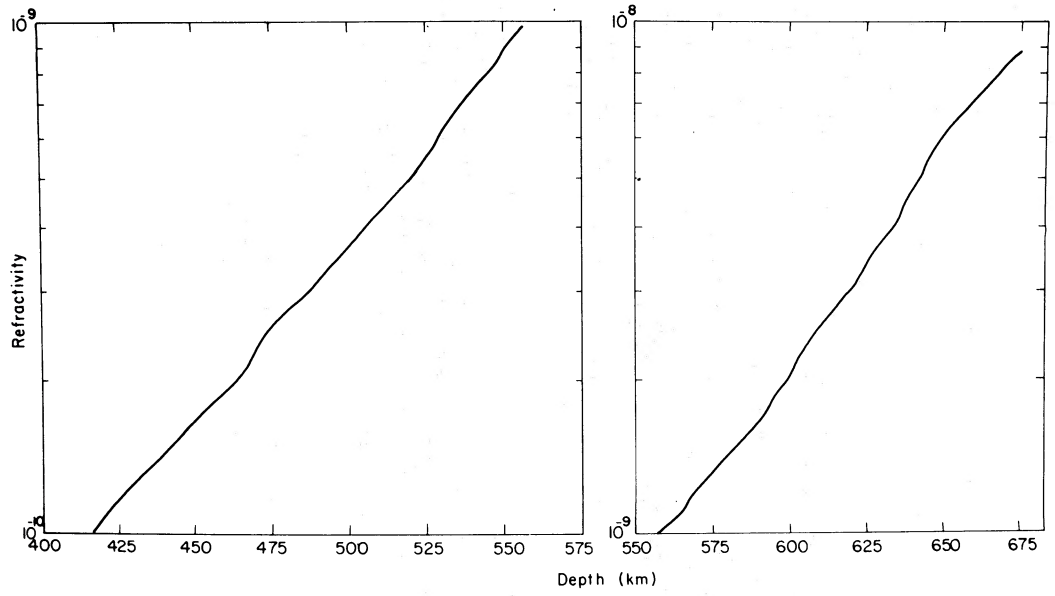

FIG. 3.—Expanded version of refractivity profile (II) shown in fig. 2. The bumps appear as spikes in the light curve. Solution I is not shown since it differs insignificantly from II at these levels (cf. fig. 2).

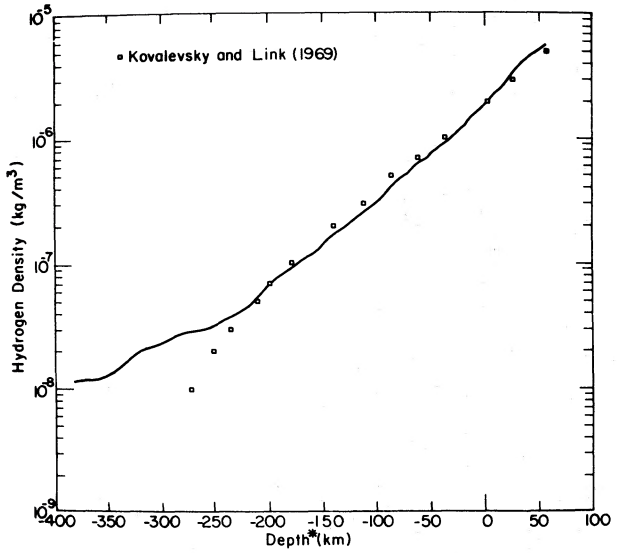

FIG. 4.—Comparison of the refractivity profile (II) derived in this paper (*solid line*) with that deduced by Kovalevsky and Link (1969) from Japanese observations of the same event (*points*). The two curves were made to coincide at a hydrogen density of 1.9×10^{-6} kg m^{-3}, and the zero of the arbitrary depth scale was shifted to this point. The asterisk after "depth" is included to underscore this shift. In all other figures the zero of the depth scale is as defined for fig. 2. The agreement with our refractivity profile (I) is even better.

Kovalevsky and Link (1969) who give not refractivities, but only density values (units not specified) for a pure hydrogen atmosphere. It seems that the density units used by Kovalevsky and Link are kg m^{-3}. On this assumption, our refractivity profile, converted to a hydrogen density profile, is compared with the emersion curve of Kovalevsky and Link in figure 4. The depth scales have been interrelated so that our value of $\rho(H_2)$ agrees with that of Kovalevsky and Link at their "mid-intensity" point, which corresponds to $\rho(H_2) = 1.9 \times 10^{-6}$ kg m^{-3}. The agreement is satisfactory, even though the Kovalevsky and Link curve is derived not from the real occultation curve, but from a "mean curve" in which spikes have been averaged out.

III. THE TEMPERATURE PROFILE

Assuming that the occultation curve samples the well-mixed region of Neptune's atmosphere below the turbopause, we can derive a temperature profile from the refractivity profiles (fig. 2) once the atmospheric composition is specified. The procedure, based on the perfect gas law and the equation of hydrostatic equilibrium, is outlined in Appendix B. Temperature profiles for the upper atmosphere of Neptune calculated from the refractivity profile are shown in figure 5 for three assumed compositions: (*a*) 100 percent H_2; (*b*) 50 percent H_2, 50 percent He by number; and (*c*) 20 percent H_2, 80 percent He by number, using both refractivity profiles I and II of figure 2.

Such temperature profiles must be interpreted with caution. First, they depend on the assumption of a well-mixed atmosphere. Second, since the refractivity profile does not converge for about 4 scale heights from the beginning of the integration, the temperature profile based on it cannot converge to the correct value for at least this distance. Therefore, the upper portions of the curves corresponding to $4\tilde{H} \sim 240$ km estimated above are not shown in figure 5. Wasserman and Veverka (1973) have demonstrated that even below this distance, very small errors in the refractivity profile translate into much larger errors in the temperature. No general error analysis can be given, but conservatively one cannot exclude the possibility of errors in the temperature profiles even below the 10^{13} cm^{-3} level. We expect, however, that below the 10^{14} cm^{-3} level the temperatures shown are accurate to better than 10 percent.

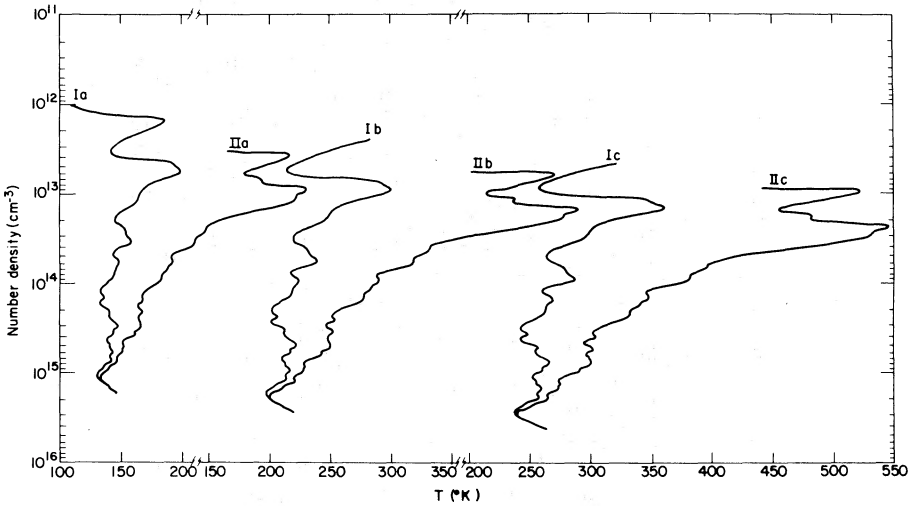

FIG. 5.—Number density versus temperature profiles for Neptune's upper atmosphere, derived from refractivity profiles I and II, for three atmospheric compositions: (*a*) 100% H_2, (*b*) 50% H_2, 50% He, and (*c*) 20% H_2, 80% He, by number. For reasons discussed in the text the upper portions of the profiles may be unreliable.

The sensitivity of the inferred temperature profiles to initial boundary conditions is emphasized by the fact that although the two refractivity profiles in figure 2 differ significantly only near the beginning of the calculation, the temperature profiles calculated from them agree closely only for the last 2 scale heights of the calculations.

The numerous bumps in the temperature profiles result from similar bumps in the refractivity profiles, which appear as spikes in the light curve. The amplitude of the temperature fluctuations is some 5°–10° K (for the 100% H_2 case), and the bumps are of the order of 10 km in vertical extent. *Under no circumstances should the upper portions of the temperature profile* $n \leqslant 10^{13}$ cm^{-3} *be given much weight.*

The fine structure of temperature profiles I and II agree closely, as do the inferred temperatures for $n \geq 10^{14}$ cm^{-3}. The overall temperature gradient inferred is quite different in the two cases. For the 100 percent H_2 model, curve I has a small positive temperature gradient of less than 0.1° K km^{-1}, whereas curve II gives 0.3° K km^{-1}. Wasserman and Veverka (1973) have shown that temperature gradients inferred in this way are subject to large systematic errors. The safest conclusion appears to be that there may be an indication of a positive temperature gradient, but that its magnitude is small. It should be recalled in this context that we have argued above that refractivity profile I should be given greater weight.

The Freeman and Lyngå analysis of this occultation curve gave $T/\mu = 38$, which means a constant temperature of 76° K for the case of a pure hydrogen atmosphere. The actual temperature profiles are nonisothermal and never reach this low value. The Kovalevsky and Link analysis of the Japanese data gives temperatures ranging from 120° to 170° K for a pure hydrogen atmosphere in the region of interest, values in general agreement with ours.

The equilibrium temperature of Neptune is less than that for Jupiter. The methane-to-hydrogen ratio is thought, both from spectroscopy (see, e.g., Freeman and Lyngå 1970, table 4) and from the mean planetary densities, to be higher on Neptune than on Jupiter. The abundance of methane photoproducts, useful in radiative cooling of planetary thermospheres, should also be greater on Neptune than on Jupiter. If no other relevant physical circumstances are significantly different, the Neptunian thermosphere should be colder than the Jovian thermosphere. The latter has been investigated by the occultation of β Sco by Jupiter, and upper limits on temperature have been derived independent of any assumption on the Jovian hydrogen-to-helium ratio (Veverka *et al.* 1974; Elliot *et al.* 1974). Comparison with figure 5 then implies that the hydrogen-to-helium number density ratio on Neptune is likely to be greater than 50 percent.

IV. DISCUSSION

In the above discussion of temperatures it was assumed that the atmospheric layers sampled by the occultation curve are well mixed. If significant amounts of He are present, the location of the turbopause becomes important, since μ will be no longer constant above the turbopause; thus the temperature algorithm in cases (*b*) and (*c*) (fig. 5) will be invalidated. The turbopause can be defined as the level at which the molecular diffusion coefficient D equals K_v, the eddy diffusion coefficient. Values of $K_v = 10^5$–10^7 cm^2 s^{-1} are often adopted for Jovian planets (McGovern and Burke 1972), from terrestrial analogy (see, e.g., Colegrove, Hanson, and Johnson 1965) while the molecular diffusion coefficient for a pure hydrogen atmosphere is given by Chapman and Cowling (1952) as

$$D \simeq 2.3 \times 10^{18}\, T^{1/2}/n \quad \text{cm}^2\,\text{s}^{-1}\,,$$

where n is the number density in cm^{-3}. To the degree of accuracy needed here, this equation can also be used for cases (*b*) and (*c*) in figure 5. To locate the turbopause, corresponding values of T and n can then be read from figure 5 and used to find D, which equals K_v at the turbopause.

In this way one finds that the turbopause will occur at $n = 10^{13}$, 10^{14}, and 10^{15} cm^{-3} for values of $K_v \simeq 3 \times 10^6$, 3×10^5, and 3×10^4 cm^2 s^{-1}, respectively. Thus, if terrestrial analogy can be used as a guide, the turbopause occurs above the 10^{14} cm^{-3} level, and the lower portions of the curves in figure 5 correspond to regions where the atmosphere is well mixed.

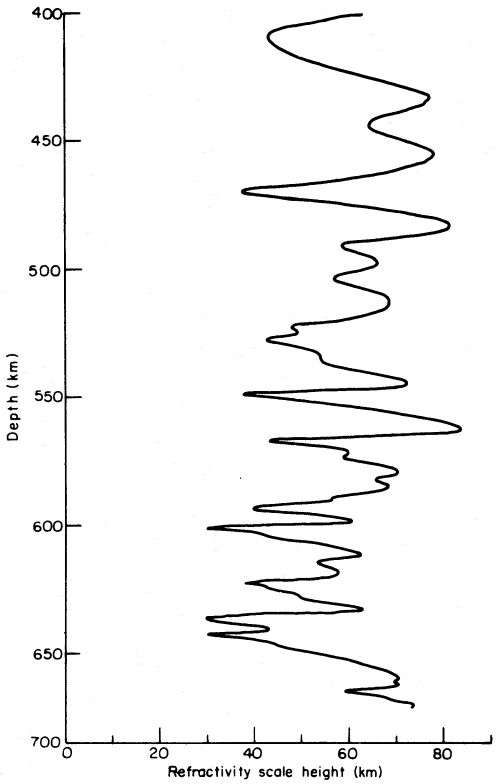

FIG. 6.—Refractivity scale height in Neptune's upper atmosphere for profile II in fig. 2. The results for profile I are closely similar.

If Neptune's atmosphere consists mostly of hydrogen, then the location of the turbopause is not important for the purposes of the temperature algorithm. Curves (*a*) in figure 5 are correct no matter where the turbopause lies. Even if large amounts of helium are present [curves (*b*) and (*c*) in fig. 5], the lower portions of the temperature curves are correct *provided* that the use of terrestrial values of K_v is justified. If the appropriate value of K_v were as low as 10^3 cm^2 s^{-1}, then our curves would be entirely above the turbopause, and in cases (*b*) and (*c*) μ would not be constant with height, so the algorithm used to generate the temperature profiles would be invalidated. Therefore, in figure 6 we have plotted the refractivity scale height H_* [where $H_*^{-1} \equiv (-1/\nu)(d\nu/dr)$] derived from curve II in figure 2; this quantity is independent of assumptions on the constancy of μ, but does illustrate the complicated structure of the upper atmosphere.

In conclusion, we reiterate the fact that uncertainties in reading chart recordings of occultation light curves can have a significant effect on inferred temperature profiles, as illustrated by the differences between solutions I and II in figure 5. It is important therefore, that all future occultation data be recorded in digital form.

We are grateful to K. C. Freeman for a facsimile of the chart recording of the emersion event, and to Kathy Rages for assistance with the analysis. We also thank P. Gierasch for helpful discussions. This work was supported in part by NASA grant NGR-33-010-082, and in part by the Atmospheric Sciences Section of the National Science Foundation grant GA 23945.

APPENDIX A

REFRACTIVITY PROFILES FROM LIGHT CURVES

The refractivity ν, at a level r in the atmosphere of a planet with radius R_p, is given by

$$\nu(r) = \frac{1}{\pi(2R_p)^{1/2}} \int_\infty^r \frac{\theta(r')dr'}{(r' - r)^{1/2}}, \qquad \text{(A1)}$$

where $\theta(r)$ is the bending of a ray whose closest distance of approach to the planet's center is r.

The coordinate system is defined such that r increases away from the planet. In addition, θ is everywhere negative, ν is everywhere positive, and $|\theta|$ and ν increase in the $-r$ direction.

Equation (A1) can be integrated by parts to give

$$\nu(r) = \frac{-2(r_1 - r)^{1/2}\theta(r_1)}{\pi(2R_p)^{1/2}} - \frac{1}{\pi(2R_p)^{1/2}} \int_{r_1}^r 2(r' - r)^{1/2} d\theta . \qquad \text{(A2)}$$

Here $r = r_1$ denotes the beginning point of the integration. Approximating the atmosphere by N spherical, concentric layers: $r_1 > r_2 > r_3 \cdots > r_N$, with $\theta_i = \theta(r_i)$ such that $|\theta_1| < |\theta_2| < \cdots < |\theta_N|$, the refractivity in the jth shell becomes

$$\nu_j = \frac{-2(r_1 - r_j)^{1/2}\theta_1}{\pi(2R_p)^{1/2}} - \frac{1}{\pi(2R_p)^{1/2}} \sum_{k=1}^{j} (r_k - r_j)^{1/2}(\theta_{k+1} - \theta_{k-1}) . \qquad \text{(A3)}$$

In this approximation, zero refractivity above the level $r = r_1$ is assumed.

The values of (r_i, θ_i) must be determined from the light-curve data points (t_i, ϕ_i). From the occultation geometry (Baum and Code 1953):

$$\left(\frac{\phi^*}{\phi} - 1\right) = D\frac{\Delta\theta}{\Delta r} \qquad \text{(A4)}$$

and

$$\Delta r + D\Delta\theta = -v\Delta t . \qquad \text{(A5)}$$

In the equations, ϕ^* = unocculted star flux; $\phi(t)$ = star flux observed at time t; D = Earth-planet distance, and v = velocity of the occultation. Equations (4) and (5) can be solved to give

$$\Delta r = -v\Delta t(\phi/\phi^*) \qquad \text{(A6)}$$

and

$$\Delta\theta = -(1 - \phi/\phi^*)v\Delta t/D . \qquad \text{(A7)}$$

Dividing the light curve into time increments $(t_1, t_2, \ldots, t_i, t_{i+1}, \ldots)$, we have, corresponding to the ith atmospheric shell,

$$\Delta t_i = t_{i+1} - t_i \quad \text{and} \quad \langle\phi_i\rangle = \tfrac{1}{2}(\phi_{i+1} + \phi_i) .$$

These values can be substituted into equations (A6) and (A7) to calculate Δr_i and $\Delta\theta_i$. The procedure is started at some point for which $\phi(t) \simeq \phi^*$, and then carried down the occultation curve, step by step, adding successive contributions to obtain

$$\theta_i = \sum_1^i \Delta\theta_i \quad \text{and} \quad r_i = \sum_1^i \Delta r_i ,$$

which are then used in equation (A3).

Ideally one should choose $r_1 \to \infty$ and $\theta_1 = \theta(r_1) \to 0$. A real occultation light curve does not extend to $r = \infty$, and the integration must start at some finite point. The assumption is made that above this level there is zero refractivity and no bending of the light. This incorrect assumption introduces an error into the calculated refractivity profile which becomes negligible 3 to 4 scale heights from the $r = r_1$ level (Wasserman and Veverka 1973). For this reason the upper portion of the refractivity profile is shown dashed in figure 2. This is the part of the solution affected by the assumed boundary condition, and

is not physically meaningful. A similar proviso applies to the temperature profile calculated from the refractivity curve. For about 4 scale heights from the beginning of the integration the inferred temperature values are influenced by errors in the refractivity profile and cannot be considered meaningful.

In addition to the height coordinate r defined above, it is convenient to define a depth coordinate z, which is measured inward, toward the planet's center, from the initial point of integration $r = r_1$.

APPENDIX B

TEMPERATURE PROFILES

To generate temperature profiles from refractivity profiles, the refractivities must first be converted to densities. For a constant atmospheric composition, the refractivity $\nu(r)$ is related to the density $\rho(r)$ by

$$\rho(r) = \frac{\rho_s}{\nu_s}\nu(r)\,, \tag{B1}$$

where the subscript s refers to standard temperature and pressure (STP) conditions.

For hydrogen/helium atmospheres, the refractivity at STP is given by

$$\nu_s = f_{\rm He}(\nu_s)_{\rm He} + f_{\rm H_2}(\nu_s)_{\rm H_2}\,,$$

where $f_{\rm He}$ = helium fraction by number and $f_{\rm H_2}$ = hydrogen fraction by number $= 1 - f_{\rm He}$. The refractivities of hydrogen and helium at STP can be approximated by

$$(\nu_s)_{\rm He} = A_{\rm He}(1 + B_{\rm He}/\lambda^2)$$

and

$$(\nu_s)_{\rm H_2} = A_{\rm H_2}(1 + B_{\rm H_2}/\lambda^2)\,,$$

where the wavelength λ is in microns and the dispersion constants, according to Brinkmann (1971), are

$$A_{\rm He} = 3.48 \times 10^{-5}\,,\quad B_{\rm He} = 2.3 \times 10^{-3}\,,$$

$$A_{\rm H_2} = 13.58 \times 10^{-5}\,,\quad \text{and}\quad B_{\rm H_2} = 7.52 \times 10^{-3}\,.$$

Once $f_{\rm He}$ is specified, the refractivity profile can be converted into a density profile from these formulae. The temperature profile can be derived from the density profile by using the perfect gas law and the equation of hydrostatic equilibrium. The atmosphere is divided into N plane-parallel layers, numbered downward 1 to N. We choose P_1 to be small, but arbitrary. The values of $\rho_1, \rho_2, \ldots, \rho_N$ are known from the light-curve inversion. The temperature structure can be found from the following set of equations:

$$\langle\rho_i\rangle = \tfrac{1}{2}(\rho_1 + \rho_{i+1})\,,\quad dP_i = -\langle\rho_i\rangle g\Delta r\,,$$

$$P_{i+1} = \sum_1 dP_i + P_1\,,\quad T_{i+1} = \frac{\mu m_{\rm H} P_{i+1}}{k\rho_{i+1}}\,. \tag{B2}$$

Here, k = Boltzmann's constant; g = acceleration due to gravity; μ = mean molecular weight; $m_{\rm H}$ = mass of a hydrogen atom; P = pressure; and T = temperature.

In the uppermost layers the temperature derived will depend significantly on the boundary condition, $P = P_1$. However, for $P_i \gg P_1$ this influence becomes negligible.

The initial value of P_1 can be taken to be zero. This initial boundary condition implies $T_1 = 0$ which is certainly not correct. A better temperature profile is obtained by iteration. A straight-line fit to a quasi-linear portion of the refractivity profile gives an approximate scale height $\tilde{H}$. If after the first iteration the pressure at level N is P_N, the next iteration begins with

$$P_1 = P_N \exp\left[-(r_1 - r_N)/\tilde{H}\right].$$

Successive iterations can be made, each time making use of $\tilde{H}$. The process converges rapidly and has been found to give good results (Wasserman and Veverka 1973). As in the case of the refractivity profile calculations, the assumed boundary condition affects the solution for about 4 scale heights ($\sim 4\tilde{H}$).

REFERENCES

Baum, W. A., and Code, A. D. 1953, *A.J.*, **58**, 108–112.
Brinkmann, R. T. 1971, *Nature*, **230**, 515–516.
Chapman, S., and Cowling, T. G. (1952). *The Mathematical Theory of Non-uniform Gases* (Cambridge: Cambridge University Press).
Colegrove, F. D., Hanson, W. B., and Johnson, F. S. 1965, *J. Geophys. Res.*, **70**, 4931–4941.
Elliot, J., Wasserman, L., Veverka, J., Sagan, C. and Liller, W. 1974, *Ap. J.* (in press).
Freeman, K. C., and Lyngå, G. 1969, *Proc. Astr. Soc. Australia*, **1**, 203–204.
Freeman, K. C., and Lyngå, G. 1970, *Ap. J.*, **160**, 767–780.
Hubbard, W. B., Nather, R. E., Evans, D. S., Tull, R. G., Wells, D. C., van Citters, G. W., Warner, B., and Vanden Bout, P. 1972, *A.J.*, **77**, 41–59.
Kovalevsky, J., and Link, F. 1969, *Astr. and Ap.*, **2**, 398–412.
McGovern, W. E., and Burk, S. D. 1972, *J. Atmos. Res.*, **29**, 179–189.
Veverka, J., Wasserman, L., Elliot, J., Sagan, C., and Liller, W. 1974, *A.J.* (in press).
Wasserman, L. H., and Veverka, J. 1973, *Icarus*, **20**, 322–345.